Research Article

Physical, magnetic and enhanced electrical properties of $SrTiO_3$–$MgFe_2O_4$ nanocomposites

Naglaa M. Sadik[1] · A. A. Sattar[1] · M. M. Rashad[2] · H. M. Elsayed[1]

Received: 16 January 2020 / Accepted: 6 March 2020 / Published online: 12 March 2020

Abstract
Multiferroic of strontium titanate and magnesium ferrite nanocomposites with chemical formula $x\ SrTiO_3 + (1-x)\ MgFe_2O_4$; $x = 0$, 0.6, 0.7, 0.8, 0.9 and 1.0 have been synthesized through sol gel auto-combustion pathway. The blending is based on ball milling method. The lattice parameters and crystallite size of the combination nanocomposites were constant with different ratios of $SrTiO_3$. FE-SEM revealed that the grain size decreased with x. The magnetization M_s was carried out using vibrating sample magnetometer at room temperature while the relative permeability μ_r was studied as a function of temperature at a constant frequency. Both saturation magnetization and relative permeability decreased with various increments of $SrTiO_3$. DC electrical resistivity and (P–E) loops measurements were investigated. The dielectric properties and DC resistivity were enhanced. Such promising results are prospective requests for sensors, high frequency applications and stage memories.

Keywords Multiferroic · $SrTiO_3$ · $MgFe_2O_4$ · Magnetic properties · Electrical properties

1 Introduction

Magnetoelectric (ME) composites, manifesting simultaneously ferroelectric and ferromagnetic characteristics, have recently been stimulated as intensive increments in a research activity. In this regard, they are considered promising materials for multifunctional devices involving energy conversion, data storage devices, transducers, actuators and magnetic sensors [1–3]. Generally, the selection of ferromagnetic/ferrimagnetic and ferroelectric materials depends on some factors, such as high magnetostrictive coefficient, high resistivity of both phases, high dielectric permittivity and high piezoelectric effect. In this context, barium titanite ($BaTiO_3$) is considered as one of the most widely used ferroelectric material for multiferroic composites [4–7]. On the other hand, the origin of ferroelectricity in $SrTiO_3$ is due to the defect engineering, which can induce the ferroelectricity in $SrTiO_3$ during the growth process of nanoparticles in a host matrix. Particularly, Sr vacancies in $SrTiO_3$ are considered as a primary source for driving the cubic-to-tetragonal structural transition necessary for ferroelectricity [8]. Kim et al. [9] demonstrated that the room temperature ferroelectricity could be produced in $SrTiO_3$ thin films. Meanwhile, S. Chintalapati et al. [10] reported that on growing of $SrTiO_3$ nanoparticles, the strain induces structural phase transition from cubic (paraelectric) to tetragonal (ferroelectric) at room temperature. It is worth mentioning that $SrTiO_3$ based multiferroic composites have previously been examined with including $Co_{0.7}Fe_{2.3}O_4$ [8], $Co_{0.8}Cu_{0.2}Fe_2O_4$ [11], and $Ni_{0.8}Zn_{0.2}\ Fe_2O_4$ [12]. Otherwise, no published works are accessible on strontium titanate ($SrTiO_3$) with magnesium ferrite ($MgFe_2O_4$) as a magnetic nanostructured material. Magnesium ferrite has high resistivity compared to other

✉ Naglaa M. Sadik, naglaa_sadik@yahoo.com; A. A. Sattar, adelsattar2@yahoo.com; M. M. Rashad, rashad133@yahoo.com | [1]Physics Department, Faculty of Science, Ain Shams University, Cairo, Egypt. [2]Advanced Materials Division, Central Metallurgical Research and Development Institute, Cairo, Egypt.

ferrites. In addition, it is considered a soft magnetic material. This property facilitates the control of electric polarization with the application of low magnetic field. So, this composite is important for potential applications in information storage, sensors, microwave devices and catalysis. Therefore, in our work, $SrTiO_3$ and $MgFe_2O_4$ nanoparticles were first synthesized by a versatile and cost-effective sol gel auto-combustion pathway based on citric acid as a fuel. Then, $MgFe_2O_4$–$SrTiO_3$ nanocomposites with various weight ratios have been elaborated through ball milling strategy. In this regard, the significant changes in structure as well as magnetic and electrical properties of the nanocomposite with different content of ferroelectric material ($x = 0$, 0.6, 0.7, 0.8, 0.9 and 1) are comprehensively investigated using different physical techniques.

2 Experimental

2.1 Sample preparation

2.1.1 Synthesis of strontium titanate nanoparticles

Strontium titanate $SrTiO_3$ nanopowder was prepared using sol–gel auto-combustion pathway. Typically, strontium nitrate tetrahydrate $Sr(NO_3)_2{\cdot}4H_2O$ and titanium(IV) ethoxide $Ti(OC_2H_5)_4$ containing 33–35% TiO_2, with molar ratio 1:1 as the starting raw materials, were dissolved in deionized water on hot plate magnetic stirrer. Then, citric acid $C_6H_8O_7{\cdot}H_2O$, which acts as a fuel to complete the reaction, was inserted into the solution with a molar ratio of 3:1:1. Further, ammonia solution was incorporated into the solution to adjust the pH value to be 9. After that, hydrogen peroxide H_2O_2 with 10% concentration was gradually added to the solution to avoid the formation of $SrCO_3$. The solution was first gently stirred at room temperature to form homogenous solution. Subsequently, the solution was heated to evaporate the water, until it dries and forms greenish gel. The obtained gel was then dried in an oven at 350 °C for 30 min. to remove the adsorbed and crystalline water and form the precursor. Finally, the dried precursor was heated at a rate of 2.5 °C min^{-1} in static air furnace at 700 °C for 4 h.

2.1.2 Synthesis of magnesium ferrite nanoparticles

Magnesium ferrite $MgFe_2O_4$ nano powder was prepared, using aqueous solutions of Fe^{3+}: Mg^{2+} with molar ratio 2:1. High purity magnesium nitrate hexahydrate $Mg(NO_3)_2{\cdot}6H_2O$ and ferric nitrate nonahydrate $Fe(NO_3)_3{\cdot}9H_2O$ were the sources of magnesium and iron. Citric acid was added to the solution with a molar ratio 3:2:1. After that, the solution was gently stirred, while being heated at 100 °C on a hot magnetic stirrer, until viscous dark brown gel was obtained. Eventually, the gel was dried at 200 °C for 8 h and then annealed in static air furnace at 400 °C for 4 h, with a heating rate of 2.5 °C min^{-1} to form the ferrite powder.

2.1.3 Formation of x $SrTiO_3$ + (1 − x) $MgFe_2O_4$ nanocomposites

$xSrTiO_3 + (1-x)\ MgFe_2O_4$ composites with x = 0,0.6, 0.7, 0.8, 0.9 and 1.0 were formed by mixing the calcined powders according to their molar ratio and grinding them using a ball milling for 1 h. The mixtures were pressed into tablets with an average thickness of 1.5 mm and a diameter of 10 mm. All samples were sintered at 400 °C for 4 h, to increase their hardness.

2.2 Physical characterization

X-ray diffraction (XRD) analysis was carried out for all investigated samples by X-ray diffractometer (X`Pert Graphics, Germany), with Cu K_α radiation of wavelength ($\lambda = 1.54056$ Å). The lattice parameter (a) and crystallite size (D) were considered, based on Rietveld refinement of XRD data.

The morphology of the samples with $x = 0$, 0.6, 0.8 and 1.0 was distinguished using Field Emission Scanning Electron microscopy (FE-SEM) (Quanta 250 FEG, Netherland) with an excitation potential of 30 kV.

The magnetic hysteresis loops were considered, at room temperature using Vibrating Sample Magnetometer (VSM;7410 Lakeshore, USA) with a maximum magnetic field of 20,000 G. The temperature dependence of relative permeability μ_r was estimated by measuring the self-inductance of a coil with and without the sample powder, using RLC bridge (TEGAM Inc. Model 3550, 42.0 Hz to 5.00 MHz) at a constant frequency of 10 kHz.

DC electrical resistivity measurement was measured on tablet samples using Fluke Digital Multi-meter (USA—model 8846 A) from room temperature up to 673 K. Surfaces of all tablet samples were polished and coated with silver paste for the electrical measurements. K type thermocouple was employed to measure the temperature.

Home-made Sawyer–Tower circuit was fabricated to investigate the P–E loops for all samples at room temperature. Maximum polarization (P_{max}) and coercive electric field (E_c) were estimated from the obtained loops.

Dielectric constant (ε′) was measured as a function of frequency with aid of LCR meter model (TEGEM 3550 LCR meter, USA).

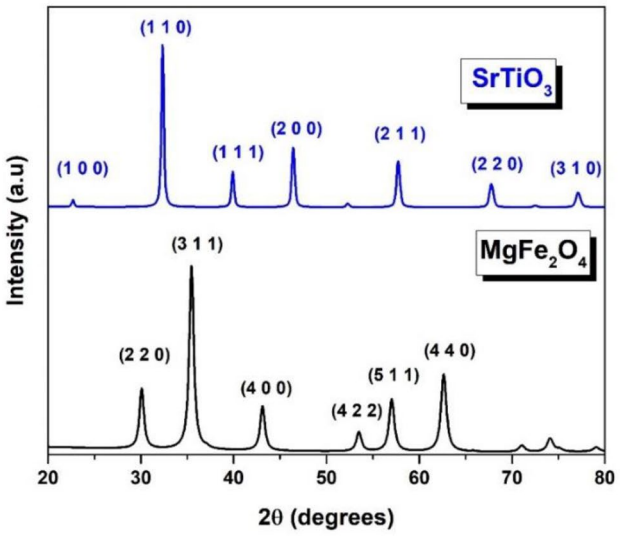

(a)

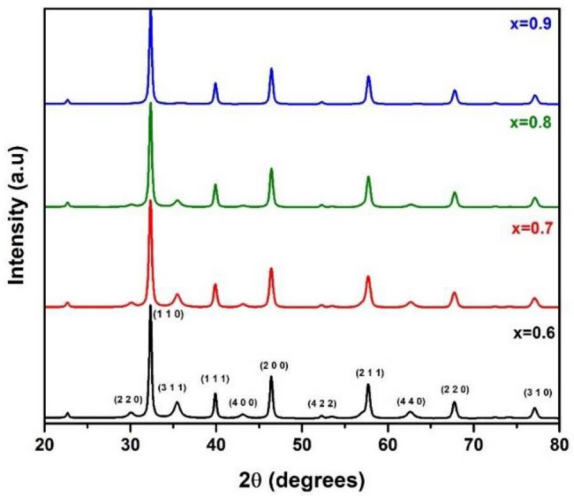

(b)

Fig. 1 XRD pattern for **a** pure $MgFe_2O_4$ and $SrTiO_3$ and **b** composite $x\ SrTiO_3 + (1-x)\ MgFe_2O_4$

3 Results and discussion

3.1 Structural analysis

Figure 1a shows the XRD diffraction profiles of synthesized $MgFe_2O_4$ and $SrTiO_3$ via sol gel auto-combustion route, based on citric acid as a fuel. Apparently, magnesium spinel ferrite with cubic structure was presented with an average lattice parameter 8.38 Å, which is in good agreement with JCPDS NO. 88-1934. Otherwise, peak positions of $SrTiO_3$ phase were confirmed with JCPDS NO. 84-443 which exhibited a cubic perovskite structure with lattice parameter 3.911 Å. Figure 1b illustrates the X-ray patterns for $MgFe_2O_4$–$SrTiO_3$ composites with $x = 0.6$, 0.7, 0.8 and 0.9. Clearly, the existence of both ferrite and ferroelectric phases, without any secondary phase, were demonstrated. It is obvious that the intensities of the ferrite phase were found to decrease with increasing the ferroelectric, until it was almost disappeared for $x = 0.9$. The variation of lattice parameter and crystallite size with ferroelectric concentration (x) is recorded in Table 1. It is obvious that the lattice parameters of both ferrite and ferroelectric phases were almost constant on increasing the ferroelectric content. Similar behavior was previously reported for $Ni_{0.90}Co_{0.05}Mn_{0.05}Fe_2O_4$–$BaTiO_3$ nanocomposite [13]. Moreover, the crystallite size of ferrite and ferroelectric phases were slightly varied with x. These results indicate that there is no interdiffusion between the two phases. Table 1 also shows that, the values of strain of ferrite increased while that of ferroelectric phase was almost stable. Similar behavior was previously reported for $Co_{0.7}Fe_{2.3}O_4$–$SrTiO_3$ [8].

3.2 Field emission scanning electron microscopy (FESEM)

FESEM images of the composites $x\ SrTiO_3 + (1-x)\ MgFe_2O_4$ with x = 0, 0.6, 0.8 and 1 are shown in Fig. 2a–d respectively. It is observed from the figures that the composites consist of mixture of white and black grains. Black grains indicate the presence of ferrite phase, while the white grains refer to the ferroelectric phase. From Fig. 2, each

Table 1 The values of lattice parameters, crystallite size, lattice strain and grain size of the system $x\ SrTiO_3 + (1-x)\ MgFe_2O_4$; x = 0, 0.6, 0.7, 0.8, 0.9 and 1

Sample	Lattice parameter (Å)		Crystallite size (nm)		Lattice strain		Grain size (nm)	
	Ferro-electric	Ferrite	Ferro-electric	Ferrite	Ferro-electric	Ferrite	Ferro-electric	Ferrite
x = 0	–	8.388	–	21	–	0.042	–	152.98
x = 0.6	3.911	8.389	49	14	0.019	0.047	75.46	109
x = 0.7	3.911	8.386	41	14	0.025	0.052	–	–
x = 0.8	3.910	8.379	45	14	0.021	0.059	47.59	40.154
x = 0.9	3.911	8.38	49	27	0.021	–	–	–
x = 1	3.910	–	56	–	0.020	–	114	–

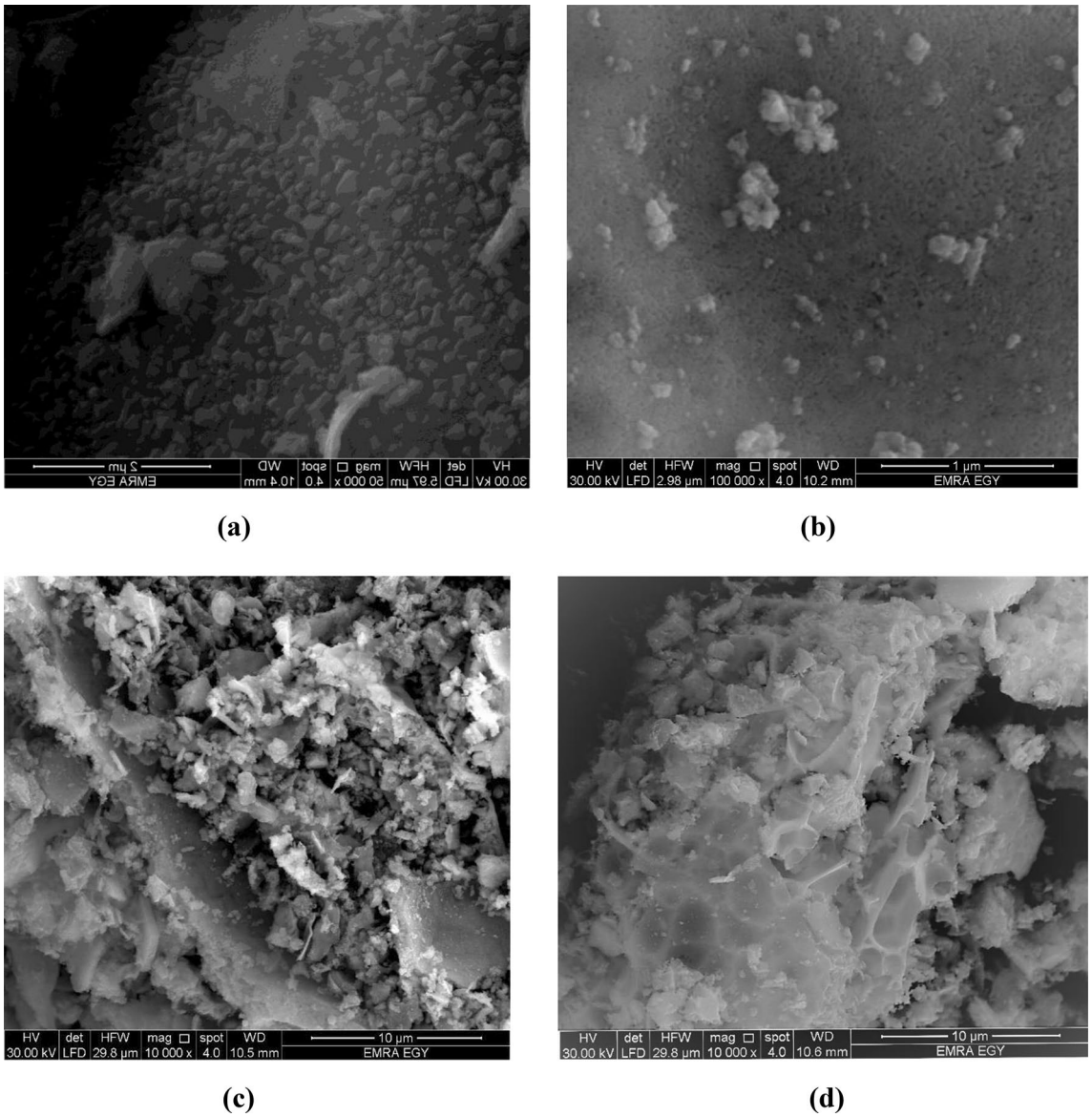

Fig. 2 FESEM images of **a** $x=0$, **b** $x=0.6$, **c** $x=0.8$ and **d** $x=1$

phase surrounds the other and causes stress on it. As the composites contain ferroelectric content higher than the ferromagnetic content so, it is expected that the stress, and the strain, on the ferromagnetic phase increases with increasing the ferroelectric concentration. On the other hand, the effect of ferrite on ferroelectric material is very small, so the strain of ferroelectric phase slightly changed, as we found experimentally. It was mentioned that, the strain in composite results from the mismatch between ferromagnetic and ferroelectric phases [14]. The average grain size is calculated by the line intercept method.

It is clear that, from Table 1, the values of grain size of pure ferrite and pure $SrTiO_3$ are large. As the percentage of $SrTiO_3$ increases in composites, the grain size of both ferroelectric material and ferrite decreases. This decrease may be because of that each phase surrounds the other, then it hinders its grain growth.

3.3 Magnetic results

Magnetic hysteresis loops of the composites with x = 0, 0.6, 0.7, 0.8 and 0.9 are shown in Fig. 3. Magnetic parameters: saturation magnetization (M_s), remanant magnetization (M_r), squareness (R) and coercivity (H_c), for each sample are listed in Table 2. These values are close to the reported values [15–17]. The value of M_s is smaller than that for bulk material [18]. The low value of M_s may be due to the small crystallite size of 14 nm which leads to the presence of

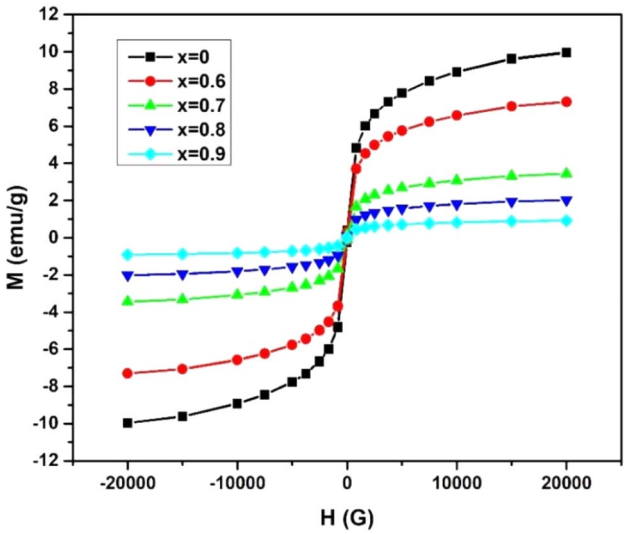

Fig. 3 Hysteresis loops for composites with different concentration *x* of $SrTiO_3$

an inactive magnetic layers or a disordered layer on the surfaces [17]. The values of M_s and M_r are decreased as ferroelectric phase increased. This decrease may be due to, the ferroelectric material is considered a non-magnetic material. So, it interrupts the exchange coupling between magnetic moments and dilutes the ferromagnetic phase [19]. Moreover, the decrease of grain size must be accompanied by a decrease of M_s and M_r. The squareness values R ($R = M_r/M_s$) as well as the coercivity (H_c) are increased as $SrTiO_3$ content increased, which is a promising property for magnetic recording systems. Our results show that, the values of R vary from 0.061 to 0.095 with increasing ferroelectric content. This means that, the inter-grain magneto static interaction across the interface between $SrTiO_3$ and $MgFe_2O_4$ increases with increasing ferroelectric content [20]. The increase of H_c may be due to the presence of the ferroelectric phase which impedes the magnetic domain rotation. Such behavior was observed for $Ni_{0.93}Co_{0.02}Mn_{0.05}Fe_{1.95}O_4$ and PZT composites [21]. The experimental magnetic moment, in Bohr magneton as shown in Table 2, was calculated for all samples according to the relation:

$$n_B(\mu_B) = \frac{M_s(emu/g) \times W(g)}{5585} \quad (1)$$

where W is the molecular weight. The crystal anisotropy constant (K) which tabulated in Table 2 is calculated from the relation [22]:

$$H_c = \frac{0.96\ K}{M_s} \quad (2)$$

According to this relation, it was expected that K increases as H_c increases. However, it was found that K decreased with x while H_c increased. In fact, K is directly proportional to the product of H_c and M_s. Looking for the magnetization dependence on x and field dependence on x, one finds that, M_s decreases much slower than H_c, i.e. increasing the ferroelectric content controls the behavior of anisotropy constant through hindering the domain motion.

Figure 4 shows the variation of relative permeability with temperature for compositions with x = 0, 0.6, 0.7 and 0.8. It can be noted that as the temperature increases, the relative permeability decreases until it reaches its minimum value. Moreover, the values of μ_r, at any temperature,

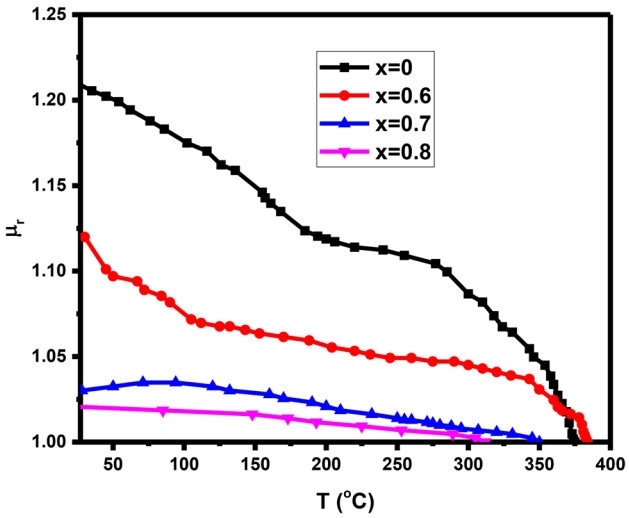

Fig. 4 Variation of relative permeability μ_r with Temperature T for *x* = 0, 0.6, 0.7 and 0.8

Table 2 The values of saturation magnetization (M_s), remenant magnetization (M_r), coercive field (H_c), squareness (R), magnetic moment (n_B) and anisotropy constant (K) for all samples

Sample	M_s (emu/g)	M_r (emu/g)	H_c (G)	$R = M_r/M_s$	n_B (μ_B)	K (erg/cm^3)
x = 0	9.97	0.33	54.18	0.061	0.36	308.71
x = 0.6	7.31	0.23	49.97	0.067	0.25	180.10
x = 0.7	3.34	0.126	58.98	0.076	0.11	97.55
x = 0.8	2.01	0.077	62.36	0.078	0.07	61.48
x = 0.9	0.91	0.046	80.9	0.095	0.03	38.912

decrease with increasing (x) exactly as M_s. This confirms that the saturation magnetization (M_s) and relative permeability (μ_r) obey Globus formula [23]:

$$\mu_r \alpha \frac{M_s^2}{K} \tag{3}$$

Physically speaking, $SrTiO_3$ acts as a dielectric material and hinders the flow of magnetic flux. Moreover, due to the large ionic radii of Sr and Ti ions, increasing of $SrTiO_3$ content (x) leads to an increasing of porosity which causes a decrease of μ_r. One notices also that the values of μ_r of nano $MgFe_2O_4$ is very small compared with the bulk ferrites due to the size effect as mentioned above. The intersection of the magnetic permeability curves of the samples with the temperature axis is called Curie temperature (T_c). Figure 5 illustrates the variation of T_c with composition x obtained from relative permeability and from DC resistivity, as will be discussed. It is obvious that the Curie temperature decreases as $SrTiO_3$ content (x) increases. The addition of higher concentration of ferroelectric phase than ferrimagnetic phase makes the ferrimagnetic phase seems as isolated islands. Hence the interactions between these islands decrease with increasing $SrTiO_3$. This statement agrees with FESEM results. Similar trend was previously reported for (x) $Ni_{0.5}Zn_{0.5}Fe_2O_4 + (1-x)$ PZT [24].

3.4 Electrical results

3.4.1 DC resistivity

Variation of DC resistivity, represented as log ρ, with reciprocal temperature (10^3/T K^{-1}) for all samples is shown in Fig. 6. It is clear that each curve could be divided into three regions, indicated on the curve of x = 0 as I, II and III. In region I the resistivity decreases gradually with increasing temperature (semiconducting behavior). In semiconductors, the carrier concentration n increases exponentially with temperature and the drift mobility μ is thermally activated [25]. The origin of increasing n results mainly from impurities such as Fe^{2+} which arise during the annealing process. The gradual decrease of ρ means that the impurities are present at different levels from the bottom of the conduction band. In region (II), the resistivity increased with temperature, metallic like behavior, which implies that in this region the temperature is not sufficient to liberate further electrons. Meanwhile the effect of lattice vibration increases with temperature, which leads the electrons to be scattered and hence an increase of resistivity [26]. In region (III), the resistivity decreased again. Comparing the temperatures at the beginning of region (III) with those of T_c determined from the relative permeability measurement as shown in Fig. 5, one can deduce that the beginning of region (III) corresponds to a ferrimagnetic-paramagnetic transition.

According to Arrhenius relation:

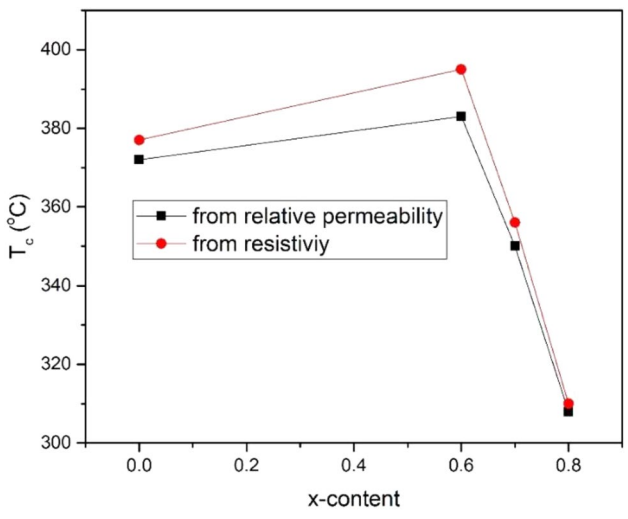

Fig. 5 Variation of Curie temperature T_c with ferro-electric content estimated from relative permeability and resistivity

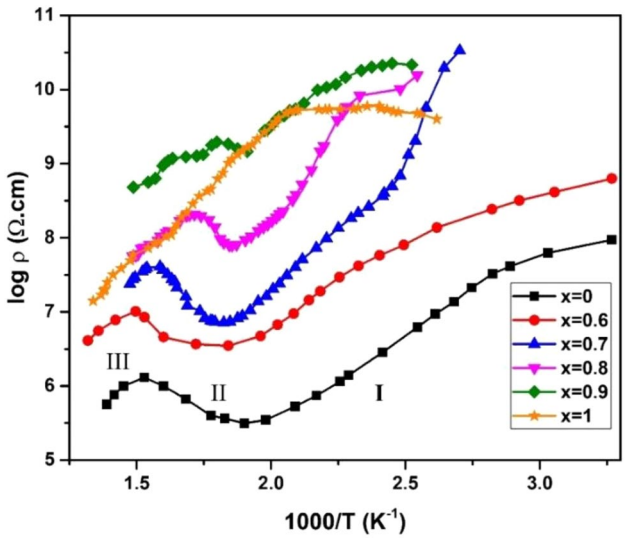

Fig. 6 Variation of resistivity with temperature for $x\ SrTiO_3 + (1-x)$ $MgFe_2O_4$

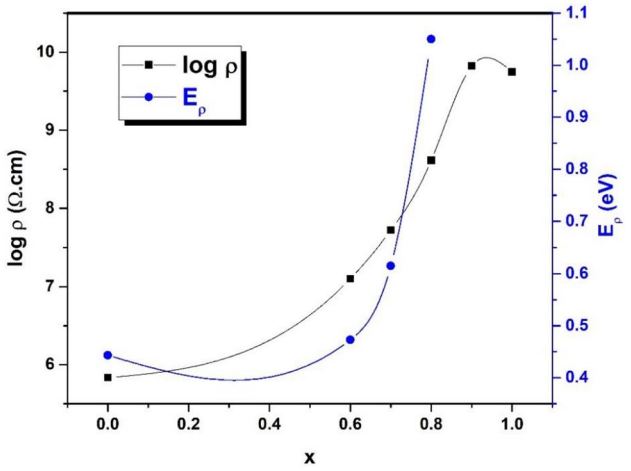

Fig. 7 Variation of DC resistivity and activation energy with ferroelectric content at T = 450 K

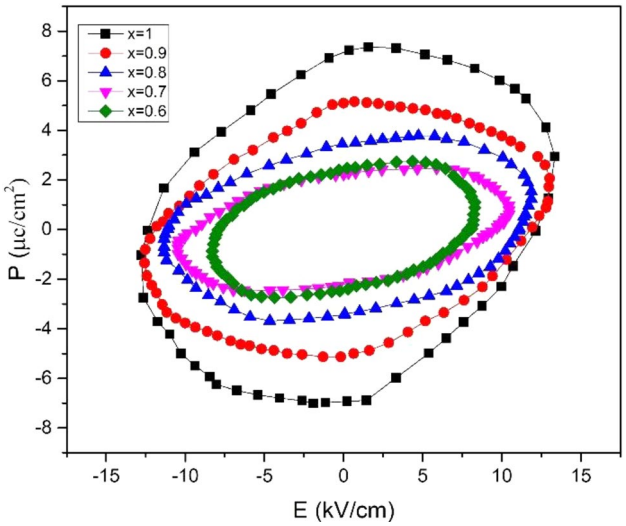

Fig. 8 P–E loops of composite with $x = 1$, 0.9, 0.8, 0.7 and 0.6

$$\rho = \rho_o \exp\left(\frac{E_\rho}{KT}\right) \tag{4}$$

We can obtain the activation energy could be obtained by plotting log ρ versus 1/*T*, the slope of the linear part (region I in Fig. 6) will be equal to (E_ρ/k). Figure 7 shows the variation of DC resistivity (log ρ) and activation energy E_ρ with ferroelectric content (x) at T = 450 K. The calculated values of activation energies are greater than 0.4 eV, which suggest that the conduction is due to hopping of charge carriers (polaron) [13]. It is obvious that, the resistivity and activation energy increase with increasing ferroelectric content (x) which satisfies the rule that high resistivity is accompanied by high activation energy. It is known that the DC resistivity of composites depends on the resistivity of the constituent phases. As the resistivity of $SrTiO_3$ is higher than that of $MgFe_2O_4$, it is expected that the values of DC resistivity of composite increase with increasing of $SrTiO_3$ content as we found experimentally. The increase in resistivity may also be attributed to the decrease in the average grain size with increasing of $SrTiO_3$ percentage. Such a decrease in grain size is accompanied by an increase of the grain boundaries in the sample which leads to an increase of the resistivity [27, 28].

3.4.2 Ferroelectric study (P–E Loops)

Figure 8 shows the room temperature (P–E) loops for the composites. Each loop is characterized by P_{max} and E_c where P_{max} is the maximum polarization and E_c is the coercive electric field. It can be seen from the figure that P–E loops are not saturated. It is due to the limited applied electric field to avoid the break down occurrence in the composite. The hysteresis loops show that the maximum polarization P_{max} increases with increasing of $SrTiO_3$, as the ferroelectric material is characterized by high polarization. Values of 7, 5.2, 3.7, 2.4 and 2 μc/cm^2 were obtained for samples with x = 1, 0.9, 0.8, 0.7 and 0.6 respectively. These values are higher than those previously reported for (1 − x) $Co_{0.7}Fe_{2.3}O_4$ − (x) $SrTiO_3$, which has a value of P_{max} = 0.3 μc/cm^2 for x = 0.75 [8] and for (1 − x) $Ba_{0.95}Sr0._{05}TiO_3$ + (x) $Ni_{0.7}Zn_{0.2}Co_{0.1}Fe_2O_4$, which has P_{max} = 2 μc/cm^2 at x = 0.1 [29]. On the other hand, E_{max} recorded a range between 8 and 12 kV/cm. This indicates that the investigated composites are being easily polarized under the effect of electric field which is important for magneto electric applications [30–32].

3.4.3 Dielectric properties with frequency

The variation of dielectric constant with frequency, 20 Hz to 5 MHz, was carried out using LCR bridge. The dielectric constant (ε′) of the samples was calculated using the relation:

$$\varepsilon' = \frac{Cd}{\varepsilon_o A} \tag{5}$$

where C (Farad) is the measured value of the capacitance of the sample, d (m) is the thickness, A (m^2) is the surface area and ε_o is the dielectric permittivity of free space (8.854×10^{-12} F/m). The variation of dielectric constant (ε′) with frequency at room temperature for all samples is shown in Fig. 9. The initial decrease in ε′ is sharp at lower frequency, then ε′ showed almost frequency independent behavior. The dispersion may be attributed by Maxwell–Wagner type of interfacial polarization [33].

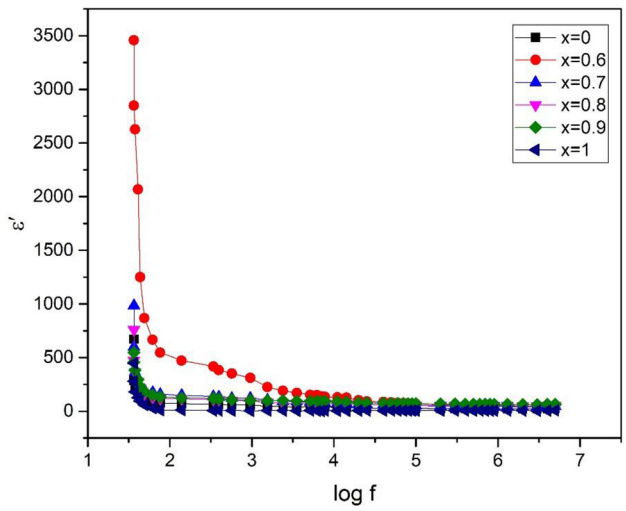

Fig. 9 Dielectric constant (ε′) versus log f at room temperature for all samples

According to Maxwell–Wagner mechanism, the composite material is supposed to consist of good conducting grains of $MgFe_2O_4$ surrounded by poor conductive grains (high resistive grain boundaries) of $SrTiO_3$. By applying an alternating electric field, charge carriers may accumulate at defects, impurity centers, voids, strains exist in the lattice and the resistive grain boundaries. This causes interfacial and space charge polarization so; the dielectric constant is high at low frequency. Further, as the frequency increases the interfacial polarization couldn't follow the field, so the interfacial polarization decreases with increasing of frequency. At higher frequency the dielectric constant becomes almost constant because the dipolar and ionic polarization couldn't follow the applied electric field. The highest value of ε′ for x = 0.6 could be attributed to the fact that the ferromagnetic regions are surrounded by nearly equal molar ratio of ferroelectric regions which rises high interfacial polarization. Dielectric properties are enhanced for all samples especially for $x = 0.6$, which has a value ε′ = 3300, while the maximum value of ε′ obtained for [(1 − x) BST + x NiZnFe] system was 1100 [34] and ε′ = 550 for [(1 − x) $NdFeO_3$–x $SrTiO_3$, x = 0.6] [35] which is a promising result for high frequency applications.

4 Conclusion

$SrTiO_3 + MgFe_2O_4$ nano composites were synthesized by sol–gel method with citric acid as a fuel. XRD revealed the presence of the ferrite and ferroelectric phases without any secondary phase. The constancy of both lattice parameters and crystallite sizes of the constituent phases confirmed the non-interdiffusion between them. Mutual strain stablished in composite due to mismatch between the two phases. Magnetization, as well as Curie temperature of the composites are found to decrease with increasing $SrTiO_3$ content. On the other hand, coercive field, electric resistivity and maximum polarization of the composites increased by increasing $SrTiO_3$. The values of activation energies showed that, the predominant conduction mechanism is due to polaron hopping. Sample with $x = 1$ showed the largest value of maximum polarization (7 μC/cm^2). Dielectric constant is enhanced for all samples especially for $x = 0.6$ which has a value ε′ = 3300. These results are promising for magnetoelectric devices and high frequency applications.

Compliance with ethical standards

Conflict of interest The authors declare that they have no competing interests.

References

1. Kulkarni SR, Kanamadi CM, Patankar KK, Chougule BK (2005) Magnetic properties and magnetoelectric effect in $Ni_{0.8}Co_{0.1}Cu_{0.1}Fe_2O_4$ + $PbZr_{0.2}Ti_{0.8}O_3$ composites. J. Mater. Sci. 40:5691–5694
2. Khader SA, Parveez A, Giridharan NV, Sankarappa T (2016) Structural, dielectric and magnetic studies of (x) $Ni_{0.7}Co_{0.1}Cu_{0.2}Fe_2O_4$ + (1 − x) $BaTiO_3$ magnetoelectric composites. AIP 1728:020573
3. Reddy NR, Ramana MV, Krishnaveni K, Kumar KVS, Murthy VRK (2007) Dielectric, elastic, anelastic and conductivity behaviour of ferroelectromagnetic composites, $Ni_{0.5}Zn_{0.5}Fe_{1.95}O_4$–δ + $Ba_{0.8}Pb_{0.2}TiO_3$. Bull Mater Sci 30:357–363
4. Tadi R, Kim Y, Sarkar D, Kim C, Ryu KS (2011) Magnetic and electrical properties of bulk $BaTiO_3$ + $MgFe_2O_4$ composite. J Magn Magn Mater 323:564–568
5. Kadam SL, Patankar KK, Mathe VL, Kothale MB, Kale RB, Chougule BK (2003) Electrical properties and magnetoelectric effect in $Ni_{0.75}Co_{0.25}Fe_2O_4$ + $Ba_{0.8}Pb_{0.2}TiO_3$ composites. Mater Chem Phys 78:684–690
6. Tan SY, Shannigrahi SR, Tan SH, Tay FEH (2011) Synthesis and characterization of composite $MgFe_2O_4$–$BaTiO_3$ multiferroic system. J Appl Phys 103:094105
7. Dzunuzovic AS, Petrovic MMV, Bobic JD, Ilic NI, Ivanov M, Grigalaitis R, Banys J, Stojanovic BD (2017) Magneto-electric properties of x$Ni_{0.7}Zn_{0.3}Fe_2O_4$ – (1 – x) $BaTiO_3$ multiferroic composites. Ceram Int 9:229
8. Gaikwad AS, Kadam RH, Shirsath SE, Wadgane SR, Shah J, Kotnala RK, Kadam AB (2018) Surprisingly high magneto-electric coupling in cubic $Co_{0.7}Fe_{2.3}O_4$–$SrTiO_3$ nanocomposites. J Alloy Compd 09:209
9. Kim YS, Yoon JKMJ, Sohn CH, Lee SB, Lee D, Jeon BC, Yoo HK, Noh TW, Bostwick A, Rotenberg E, Yu J, Bu SD, Mun BS (2014) Impact of vacancy clusters on characteristic resistance change of non-stoichiometric strontium titanate nano-film. AIP 104:013501
10. Chintalapati S, Shen L, Xiong Q, Feng YP (2015) Magnetism in phosphorene: interplay between vacancy and strain. AIP 107:072401

11. Ahmed MA, Mansour SF, Abdo MA (2013) Improvement of the physical properties of novel (1 − y) $Co_{0.8}Cu_{0.2}Fe_2O_4$ + (y) $SrTiO_3$ nanocomposite. Mater Res Bull 48:1796–1805
12. Yang H, Wang H, Xiang WF, Yao X (2009) Microstructure and electromagnetic properties of $SrTiO_3$/$Ni_{0.8}Zn_{0.2}Fe_2O_4$ composites by hybrid process. J Am Ceram Soc 92:1551–2916
13. Lokare SA, Khollam YB (2015) Structural and electrical properties of (1 − x) $Ni_{0.9}Co_{0.05}Mn\ Fe_2O_4$ + (x) $BaTiO_3$ magnetoelectric composites. IJCPS 4:2319–6602
14. Bangruwa JS, Vashisth BK, Singh N, Verma V (2018) Anomalous ferroelectric and magnetic behavior in BPFO–NZFO multiferroic nanocomposites. Ceram Int 44:11737–11744
15. Naseri MG, Ara MHM, Saion EB (2014) Superparamagnetic magnesium ferrite nanoparticles fabricated by a simple, thermal-treatment method. J Magn Magn Mater 350:141–147
16. Maensiri S, Sangmanee M, Wiengmoon A (2009) Magnesium ferrite ($MgFe_2O_4$) nanostructures fabricated by electrospinning. Nanoscale Res Lett 4:221–228
17. Naseri MG, Saion EB, Ahangar HA, Hashim M, Shaari AH (2011) Synthesis and characterization of manganese ferrite nanoparticles by thermal treatment method. J Magn Magn Mater 323:1745–1749
18. Gaikwad BR, Khirade PP, Kurmude DV, Shinde AB, Pandit AA, Jadhav KM (2013) Comparative study of the structural and magnetic properties of magnesium ferrite prepared by ceramic and sol–gel auto combustion technique. J App Cem 5:1275–1280
19. Bammannavar BK, Chavan GN, Naik LR, Chougule BK (2009) Magnetic properties and magnetoelectric (ME) effect in ferroelectric rich $Ni_{0.2}Co_{0.8}\ Fe_2O_4$ + $PbZr_{0.8}Ti_{0.2}O_3$ ME composites. Mater Chem Phys 117:46–50
20. Ahmed MA, Okasha N, Hussein B (2012) Enhancement of the magnetic properties of Al/La multiferroic. J Magn Magn Mater 324:2349–2354
21. Babu SN, Suryanarayana SV, Bhimasankaram T (2009) Magnetic and magnetoelectric characterization of $Ni_{0.93}Co_{0.02}Mn_{0.05}Fe_{1.95}O_4$ and PZT composites. J Alloys Compd 473:418–422
22. Stoner EC, Wohlfarth EP (1948) A mechanism of magnetic hysteresis in heterogeneous alloys. Philos Trans R Soc A Math Phys Eng Sci 240:599–642
23. Globus A, Duplex P, Guyot M (1971) Determination of initial magnetization curve from crystallites size and effective anisotropy field. IEEE Trans Magn 7:617–622
24. Bammannavar BK, Naik LR (2012) Study of magnetic properties and magnetoelectric effect in (x) $Ni_{0.5}Zn_{0.5}Fe_2O_4$ + (1 − x) PZT composites. J Magn Magn Mater 324:944–948
25. Mulushoa SY, Murali N, Wegayehu MT, Margarette SJ, Samatha K (2018) Influence of Cu–Cr substitution on structural, morphological, electrical and magnetic properties of magnesium ferrite. Res Phys 8:772–779
26. Pillai SO (2010) Solid state physics, 6th edn. New Age International (P) Limited Publishers, New Delhi, pp 558–560
27. Jadhav PA, Shelar MB, Chougule SS, Chougule BK (2010) Structural, electrical conduction and magnetoelectric properties of y ($Ni_{0.3}Cu_{0.4}Zn_{0.3}Fe_2O_4$) + (1 − y) [50%$BaTiO_3$ + 50% PZT] ME composites. Phys B 405:857–861
28. Kadam SL, Patankar KK, Kanamadi CM, Chougule BK (2004) Electrical conduction and magnetoelectric effect in $Ni_{0.50}Co_{0.50}Fe_2O_4$ + $Ba_{0.8}Pb_{0.2}TiO_3$ composites. Mater Res Bull 39:2265–2272
29. Sharma R, Singh V, Kotnala RK, Tandon RP (2015) Investigation on the effect of ferrite content on the multiferroic properties of (1 − x) $Ba_{0.95}Sr_{0.05}TiO_3$ − (x) $Ni_{0.7}Zn_{0.2}Co_{0.1}Fe_2O_4$ ceramic composite. Mater Chem Phys 160:447–455
30. Peng J, Hojamberdiev M, Li H, Mao D, Zhao Y, Liu P, Zhou J, Zhu G (2015) Electrical, magnetic, and direct and converse magnetoelectric properties of (1 − x)$Pb(Zr_{0.52}Ti_{0.48})O_3$ − (x)$CoFe_2O_4$ (PZT–CFO) magnetoelectric composites. J Magn Magn Mater 378:298–305
31. Praveena K, Varma KBR (2014) Enhanced electric field tunable magnetic properties of lead-free $Na_{0.5}Bi_{0.5}TiO_3$–$MnFe_2O_4$ multiferroic composites. J Mater Sci Mater Electron 25:5403–5409
32. Wang Y, Wang Y, Rao W, Wang M, Li G, Li Y, Gao J, Zhou W, Yu J (2012) Dielectric, ferromagnetic and ferroelectric properties of the (1 − x) $Ba_{0.8}Sr_{0.2}TiO_3$–x $CoFe_2O_4$ multiferroic particulate ceramic composites. J Mater Sci Mater Electron 23:1064–1071
33. Maxwell JC (1892) A treatise on electricity and magnetism. Oxford University Press, London, p 828
34. Mondal RA, Murty BS, Murthy VRK (2015) Dielectric, magnetic and enhanced magnetoelectric response in high energy ball milling assisted BST-NZF particulate composite. Mater Chem Phys 167:338–346
35. Murtaza T, Khan MS, Ali J, Hussain T, Asokan K (2018) Structural, electrical and magnetic properties of multiferroic $NdFeO_3$–$SrTiO_3$ composites. J Mater Sci Mater Electron 29:18573–18580